

Comprehensive Pyro-Phototronic Effect Enhanced Ultraviolet Detector with ZnO/Ag Schottky Junction

Ying Wang, Laipan Zhu, Yunjie Feng, Zhaona Wang,* and Zhong Lin Wang*

As a coupling effect of pyroelectric and photoelectric effect, pyro-phototronic effect has demonstrated an excellent tuning role for fast response p–n junction photodetectors (PDs). Here, a comprehensive pyro-phototronic effect is utilized to design and fabricate a self-powered and flexible ultraviolet PD based on the ZnO/Ag Schottky junction. By using the primary pyroelectric effect, the maximal transient photoresponsivity of the self-powered PDs can reach up to 1.25 mA W^{-1} for 325 nm illumination, which is improved by 1465% relative to that obtained from the steady-state signal. The relative persistent secondary pyroelectric effect weakens the height of Schottky barrier, leading to a reduction of the steady-state photocurrent with an increase in the power density. When the power density is large enough, the steady-state photocurrent turns into a reverse direction. The corresponding tuning mechanisms of the comprehensive pyro-phototronic effect on transient and steady-state photocurrent are revealed based on the bandgap diagrams. The results may help us to further clarify the mechanism of the pyro-phototronic effect on the photocurrent and also provide a potential way to optimize the performance of self-powered PDs.

attentions and become a very important research topic in the field of UV detection.^[3] As a typical wide bandgap material, zinc oxide (ZnO) has the characteristics of large exciton binding energy ($\approx 60 \text{ meV}$), small electron and hole collision ionization coefficient, environmental friendliness, and the chemical and radiation hardness.^[4–6] As a result, ZnO is expected to realize the room temperature UV detector with high signal-to-noise ratio. And lots of ZnO-based UV photodetectors (PDs) have been designed and fabricated based on the photovoltaic effect and/or photoconductive effect.^[7–9] To satisfy the increasing demand of flexible and intelligent photosensing in wearable electronics,^[10,11] smart sensors,^[12,13] and optoelectronics,^[14–16] the self-powered ZnO-based PDs^[17] have been implemented by using the photovoltaic effect due to the internal electric field inside the Schottky junction^[18,19] and p–n junction.^[20,21] Considering the advantages of low cost, simple fabrication, and relative fast response of Schottky junction,^[22] many UV detectors with fast response are achieved based on this type of metal/semiconductor contact.^[9,17,18,23] But the relatively weak intrinsic internal electric field in Schottky junction makes this self-powered PD demonstrate relative low photoresponsivity which hinders its further practical applications.^[24] Therefore, it is necessary to find a way to effectively improve the performances of the self-powered PDs with Schottky contact.

Fortunately, pyro-phototronic effect is proposed to improve the performances of the ZnO-based PDs by naturally coupling the light-induced pyroelectric effect, photonic excitations, and semiconductor properties.^[25] The light-induced pyroelectric polarization charges in wurtzite-structured ZnO nanowires (NWs) upon illumination can effectively modulate/tune the carrier generation, separation, transportation, and recombination within the p–n junction. And this interfacial physical effect can be used as an effective approach to enhance the performances of the self-powered PDs from UV to near-infrared.^[26–28] By utilizing the pyro-phototronic effect, the UV PDs with fast response and relative high photoresponsivity have been proposed based on the p–n heterojunction structures on a hard substrate.^[29] However, the total pyroelectric effect is greatly affected by the holding states, which can be divided into the primary pyroelectric effect and the secondary pyroelectric effect (thermal strain effect).^[30–32] When the sample is subjected to a constant strain (for example, a hard substrate), the

performances of the self-powered PDs from UV to near-infrared.^[26–28] By utilizing the pyro-phototronic effect, the UV PDs with fast response and relative high photoresponsivity have been proposed based on the p–n heterojunction structures on a hard substrate.^[29] However, the total pyroelectric effect is greatly affected by the holding states, which can be divided into the primary pyroelectric effect and the secondary pyroelectric effect (thermal strain effect).^[30–32] When the sample is subjected to a constant strain (for example, a hard substrate), the


1. Introduction

Due to high anti-interference ability, ultraviolet (UV) detection technology has potential applications in military detection, environmental monitoring, flame warning, life science, and astronautics.^[1,2] In particular, the wide bandgap semiconductor-based UV detector has the advantages of simple structure, easy miniaturization and integration, and good robustness for radiations and severe environment. It has attracted plenty of

Y. Wang, Y. Feng, Prof. Z. Wang
Department of Physics
Applied Optics Beijing Area Major Laboratory
Beijing Normal University
Beijing 100875, China
E-mail: zhnwang@bnu.edu.cn

Dr. L. Zhu, Prof. Z. L. Wang
Beijing Institute of Nanoenergy and Nanosystems
Chinese Academy of Sciences
Beijing 100083, China
E-mail: zhong.wang@mse.gatech.edu

Prof. Z. L. Wang
School of Materials Science and Engineering
Georgia Institute of Technology
Atlanta, GA 30332-0245, USA

 The ORCID identification number(s) for the author(s) of this article can be found under <https://doi.org/10.1002/adfm.201807111>.

DOI: 10.1002/adfm.201807111

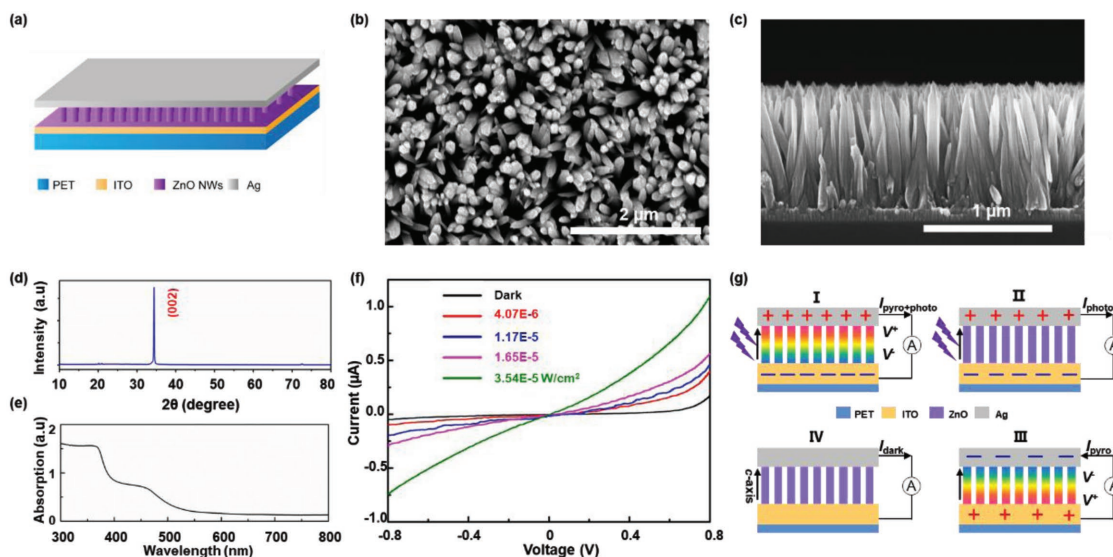


Figure 1. Design of the self-powered ZnO/Ag Schottky junction PD enhanced primarily by the pyro-phototronic effect. a) Schematic demonstration of the structure of the self-powered ZnO/Ag Schottky junction PD. b,c) SEM images of ZnO NWs array: side view b) and top view c). d) XRD spectra of ZnO NWs layer on the glass. e) Absorption spectra of ZnO NWs layer. f) I - V characteristics of the pyro-phototronic-effect-based PD under dark and 325 nm laser illumination with different power densities. g) Systematical illustration of working mechanism of the pyro-phototronic effect on the transient current in a complete chopper period to UV illumination.

primary pyroelectric effect is mainly exhibited as the previous reports.^[26–28] When the sample is subjected to a constant stress (such as a soft substrate), the secondary pyroelectric effect cannot be neglected. Thus, it is very important to investigate the tuning principle of comprehensive pyro-phototronic effect on the output current when the Schottky PDs are fabricated on flexible substrates.

In this work, a self-powered UV PD with ZnO/Ag Schottky contact is proposed on a flexible substrate via simple processes of hydrothermal synthesis and magnetron sputtering. The dynamic response characteristics of the fabricated detector are systematically investigated based on the comprehensive pyro-phototronic effect. By increasing the power density of UV light, the primary pyroelectric effect in ZnO NWs is increased, resulting in the transient photocurrent increase. Meanwhile, the secondary pyroelectric effect is also observed by sustained modifying the height of the Schottky barrier, leading to the steady-state photocurrent decrease and even turning into a reverse direction with increasing the power density. By using the comprehensive pyro-phototronic effect, the transient photo-current is improved by 10–156% relative to the steady-state photocurrent under a power density of $4.98 \times 10^{-4} \text{ W cm}^{-2}$. The results not only further clarify the mechanism of pyro-phototronic effect on the photocurrent in Schottky junction detectors, but also put forward the practical applications of ZnO-based PDs in UV imaging, environmental monitoring, and flame warming as a self-powered device.

2. Results and Discussions

Considering the forming condition of Schottky contact and the work function of ZnO,^[33,34] the metal Ag is used as an electrode to collect the free carriers and form ZnO/Ag Schottky contact.

The structure of the self-powered PD is schematically illustrated in Figure 1a and Figure S1 in the Supporting Information. A flexible polyethylene terephthalate (PET) is washed by deionized (DI) water and alcohol, then dried at room temperature, followed by sequentially sputtering a layer of indium tin oxide (ITO) as the bottom electrode and a thin layer of ZnO (100 nm) as the seed layer for ZnO NW growing. ZnO NW array is then synthesized via a low-temperature hydrothermal method. The side-view and top-view scanning electron microscopy (SEM) images of ZnO NWs are presented in Figure 1b,c, respectively, indicating ZnO NWs with an average diameter of 100 nm and an average length of 1 μm . The crystal structure of ZnO NWs on the commercial glass is characterized by X-ray diffraction (XRD) as exhibited in Figure 1d. It can be clearly identified that the preferred orientation of the NW array is almost along the c -axis (002).

The absorption spectrum of ZnO NWs in Figure 1e exhibits an obvious bandgap absorption for the light with the wavelength below 370 nm and the weak defect absorption near 450 nm. I - V curves of the ZnO-based PD without/under 325 nm laser illumination are measured and plotted in Figure 1f, showing good UV response when the device is biased at the positive or negative voltages. In the dark, the fabricated PD exhibits a good rectifying behavior as shown in Figure 1f (black line), indicating that a Schottky contact between ZnO NWs and Ag electrode is formed. Under 325 nm illumination, the output currents increase monotonously as increasing the power density under each bias voltage. When the Ag electrode is biased at 0.8 V, the output current increases from 0.17 (dark) to 1.1 μA for UV illumination with a power density of $3.54 \times 10^{-5} \text{ W cm}^{-2}$ in Figure S2 in the Supporting Information.

The working mechanism of primary pyro-phototronic effect induced by the primary pyroelectric effect in the Schottky junction is illustrated in Figure 1g, containing four-stage physical

processes similar to that of the p–n junction detector.^[35] In stage “I,” UV illumination instantaneously increases the temperature of ZnO NWs and then induces the pyroelectric polarization charges across the ZnO NWs with positive transient pyro-potential at the Ag electrode side, and negative transient pyro-potential at the ITO electrode side. Combining with the photovoltaic effect within the Schottky junction, the output signals with a sharp rising edge are thus observed at the moment of turning on light, demonstrating the photocurrent flowing from Ag to ITO electrode through the external circuit. The corresponding short-circuit current is labeled as $I_{\text{pyro+photo}}$. In stage “II,” the illumination is stable and the temperature stays at constant. As a result, the transient pyroelectric potential induced by the primary pyroelectric effect disappears rapidly due to the lack of temperature difference, and the output current decays to a stable plateau through the external circuit, labeled as I_{photo} . In stage “III,” the illumination is eliminated and the common photocurrent disappears, while an instantaneous temperature reduction results in a pyro-potential distribution in the opposite direction to that in stage “I,” leading to a transient external current labeled as I'_{pyro} flows from ITO to Ag electrode as a reverse current peak. In stage “IV,” the temperature falls back to room temperature and stays steady, and the output returns to dark current I_{dark} .

The dynamic response of ZnO/Ag Schottky junction PDs to 325 nm illuminations is systematically investigated and summarized in Figure 2a by varying the power densities from 1.22×10^{-5} to $7.48 \times 10^{-4} \text{ W cm}^{-2}$. Obviously, four-stage photocurrent dynamic behavior induced by the pyro-phototronic effect is observed at all the power densities under a zero-bias voltage. The corresponding currents $I_{\text{pyro+photo}}$ and I_{photo} are extracted and plotted in Figure 2b as black and red dots, respectively, to demonstrate the output signals of ZnO/

Ag Schottky junction PDs enhanced by the comprehensive pyro-phototronic effect. With increasing the power density, the transient short-circuit currents $I_{\text{pyro+photo}}$ increase, while the steady-state current I_{photo} first slightly increase and then decrease which is different from the traditional variation behaviors of response current increasing with power density.^[25,36,37] Besides, the enhancement factor of $E_1 = |(I_{\text{pyro+photo}} - I_{\text{photo}}) / I_{\text{photo}}|$ first increases and then decreases with increasing the power density, demonstrating a maximum value of ≈ 10 156% at $4.98 \times 10^{-4} \text{ W cm}^{-2}$ as shown in Figure S3a in the Supporting Information. The large enhancement factor indicates that the comprehensive pyro-phototronic effect can greatly improve and/or even optimize the performances of the Schottky junction PDs.

To understand the enhancement role of comprehensive pyro-phototronic effect on the performances of ZnO/Ag Schottky junction PDs, the corresponding photoresponsivity is calculated as $R = \frac{I_{\text{light}} - I_{\text{dark}}}{P_{\text{ill}}}$,^[38] where I_{light} and I_{dark} represent the short-circuit current with and without illumination, respectively. $P_{\text{ill}} = I_{\text{ill}} \times S$ is defined as the effective illumination power on the PDs, where I_{ill} is the excitation power density and S is the effective area of the PDs. The corresponding photoresponsivity $R_{\text{pyro+photo}}$ and R_{photo} are calculated and summarized in Figure 2c under each power density. The transient $R_{\text{pyro+photo}}$ first increases then decreases with increasing the power density, showing a maximum of $\approx 1.25 \text{ mA W}^{-1}$ at a power density of $3.8 \times 10^{-5} \text{ W cm}^{-2}$. Interestingly, the stable R_{photo} demonstrates monotonous reduction trend with the power density. By introducing the comprehensive pyro-phototronic effect, the photoresponsivity $R_{\text{pyro+photo}}$ are dramatically enhanced with a maximum enhancement factor $E_R = |(R_{\text{pyro+photo}} - R_{\text{photo}}) / R_{\text{photo}}|$ of 8371% at a power density of $4.98 \times 10^{-4} \text{ W cm}^{-2}$ as shown in Figure S3b in the Supporting Information. Similarly, the corresponding specific detectivity is calculated

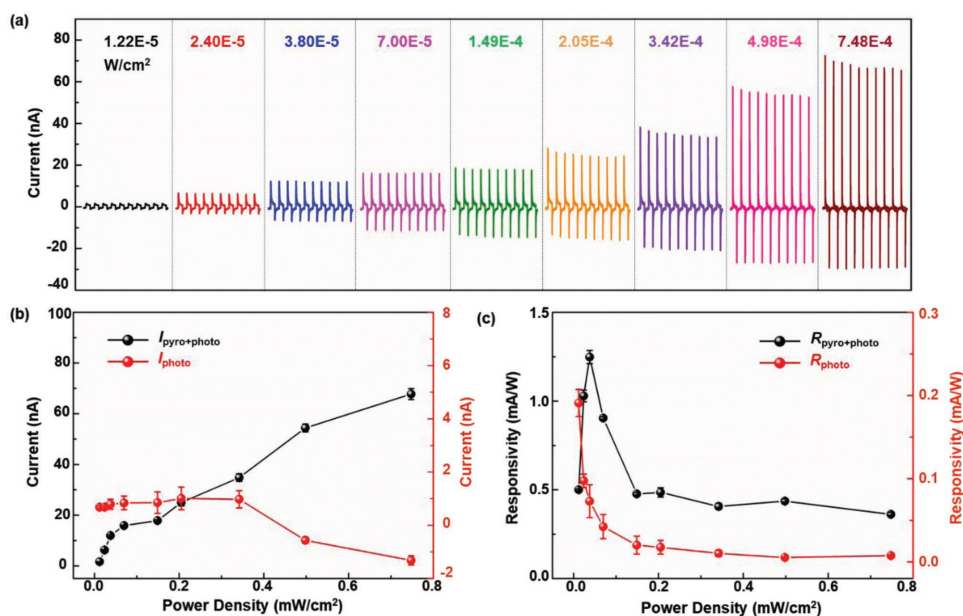


Figure 2. Pyro-phototronic effect enhanced performances of the self-powered ZnO/Ag Schottky junction PD. a) I – t characteristics of pyro-phototronic effect-based PD under 325 nm illuminations with different power densities from 1.22×10^{-5} to $7.48 \times 10^{-4} \text{ W cm}^{-2}$. b) The transient short-circuit current $I_{\text{pyro+photo}}$ and the steady-state current I_{photo} as a function of the power density. c) The corresponding photoresponsivity $R_{\text{pyro+photo}}$ and R_{photo} as a function of the power density.

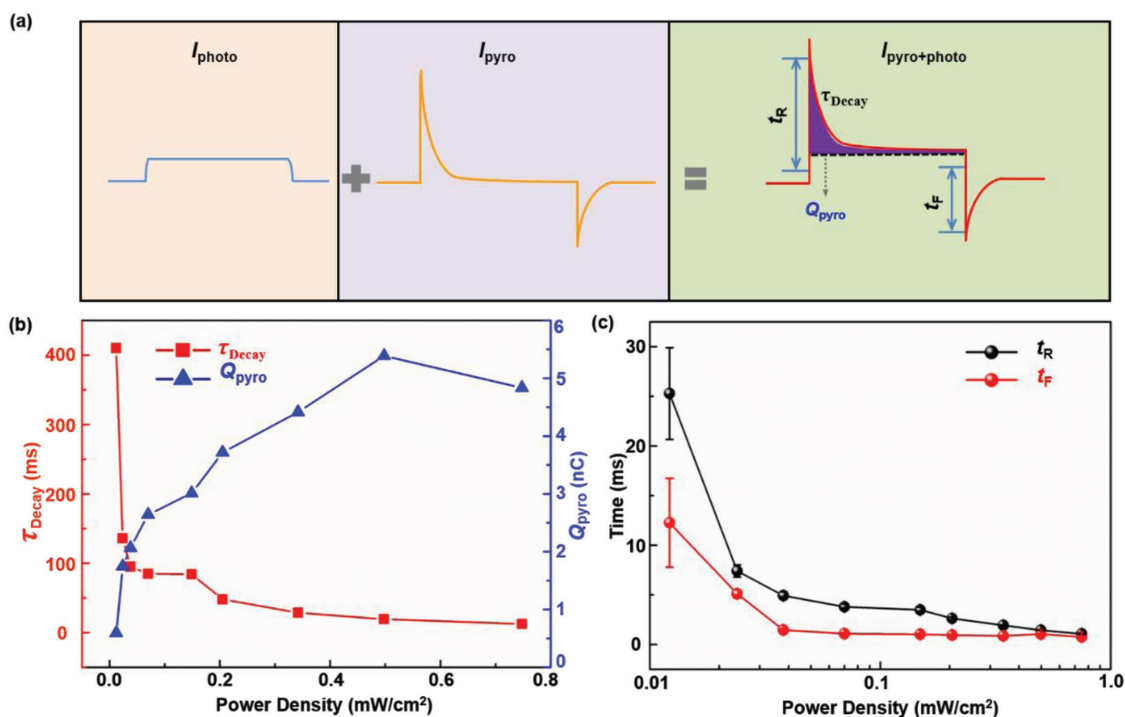


Figure 3. Time response characteristics of the pyro-phototronic-effect-based ZnO/Ag Schottky junction PD. a) Schematic demonstration of the transient photocurrent response of self-powered PD induced by photo-pyroelectric effect via combination of photovoltaic effect and pyroelectric effect. b,c) The decay time constants and pyroelectric polarization charges Q_{pyro} of the self-powered PD b) and the corresponding response time including rise time and fall time c) under different power densities from 1.22×10^{-5} to $7.48 \times 10^{-4} W cm^{-2}$.

as $D^* = R/(2q \cdot I_{dark}/S)^{0.5}$ to represent the smallest detectable signal by considering the dark current I_{dark} as major noise.^[39] The corresponding specific detectivity $D^*_{pyro+photo}$ and D^*_{photo} demonstrate a similar regular to that of photoresponsivity with the power density in Figure S4 in the Supporting Information, presenting a maximum of 2.7×10^9 Jones. The results indicate the great potential applications of pyro-phototronic effect in optoelectronic devices.

To further reveal the physical mechanism of comprehensive pyro-phototronic effect, the dynamic photocurrent response of self-powered ZnO/Ag Schottky junction PD is shown in Figure 3a by extracting the photovoltaic effect and pyro-phototronic effect. Under the illumination, the photocurrent is induced by naturally coupling a relative slow process of photovoltaic effect and a fast physical process of primary pyro-phototronic effect in Schottky junction. As a result, the transient current $I_{pyro+photo}$ is induced by photovoltaic effect and pyro-phototronic effect, and the steady-state current I_{photo} is mainly caused by the photovoltaic effect. The amount of transferred charges Q_{pyro} driven by the pyroelectric effect is thus approximately obtained by integrating the $I-t$ curve above the reference value I_{photo} . Time constant τ_{Decay} from the transient peak current $I_{pyro+photo}$ transiting to the steady-state current represents the decay process of the primary pyro-phototronic effect through the external circuit. Pyroelectric charges Q_{pyro} and decay time constant τ_{Decay} are calculated and investigated under various power densities as shown in Figure 3b. The time constant τ_{Decay} decreases with increasing the power density, attributing to the electric time constant reduction for the

whole device due to the photogenerated carriers significantly decreasing the resistivity of the semiconductor.^[40,41] While a maximal value of pyroelectric charge quantity Q_{pyro} is observed as 5.39 nC under a power density of $4.98 \times 10^{-4} W cm^{-2}$. The maximum of Q_{pyro} is attributed to the simultaneously existing competition between the enhancement role of the comprehensive pyro-phototronic effect as an increasing manner in $I_{pyro+photo}$ and the photogenerated carriers induced decreasing behavior in decay constant τ_{Decay} upon illumination.

The response time of the self-powered PD to 325 nm illuminations is also calculated and shown in Figure 3c by defining the time of the current increasing from 10% to 90% and decreasing from 90% to 10% of the maximum photocurrent, respectively. When the PD is under zero bias, both rise time t_R and fall time t_F decrease sharply with increasing the power density from 1.22×10^{-5} to $7.84 \times 10^{-4} W cm^{-2}$, demonstrating a similar behavior to that of p-n junction PDs.^[25] Figure S5 in the Supporting Information shows the pyro-phototronic effect enhancements on response speed of ZnO/Ag Schottky junction PDs by comparing rise time and fall time under the bias voltages of 0 and 0.04 V at a power density of $3.68 \times 10^{-4} W cm^{-2}$. The rise time and fall time are significantly decreased from ≈ 318.9 to 4.5 ms and from ≈ 780.3 to 3.5 ms, respectively. These results indicate over 6900% and 22 000% improvements on rise time and fall time by the comprehensive pyro-phototronic effect, respectively.

To well reveal the tuning role of the comprehensive pyro-phototronic effect on the steady-state current, the dynamic response characteristics of the ZnO/Ag Schottky junction PD are

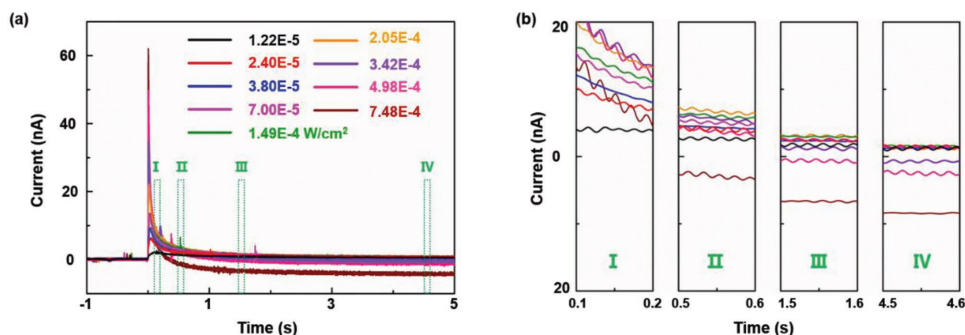


Figure 4. Dynamic characteristics of the ZnO/Ag Schottky junction PD enhanced by the pyro-phototronic effect. a) $I-t$ dynamic response characteristics of the flexible self-powered PD under 325 nm illuminations with different power densities from 1.22×10^{-5} to $7.84 \times 10^{-4} \text{ W cm}^{-2}$. b) The amplification of regions I, II, III, and IV in a).

depicted in **Figure 4a** by varying the power densities of 325 nm lasing from 1.22×10^{-5} to $7.84 \times 10^{-4} \text{ W cm}^{-2}$. It is obvious that the transient short-circuit current $I_{\text{pyro+photo}}$ increases while I_{photo} first increases and then decreases with the power density. All the transient currents go through a decay process to a steady-state current with a different speed due to the different decay time constants under different power densities as shown in **Figure 3b**. And the corresponding time-slice curves is shown in **Figure 4b** to carefully demonstrate the whole evolutionary process of short-circuit currents. During the decay process, the external circuit currents are all from Ag to ITO at the initial time of 0.1–0.2 s (region “I”). Afterward, the current induced by strong UV light at a power density of $7.84 \times 10^{-4} \text{ W cm}^{-2}$ turns into a reverse direction as shown in the time region “II.” After a long decay time, the currents I_{photo} will be stable to a positive

or negative constant in the time regions of “III” and “IV.” The stable current first increases then decreases to a negative value with increasing the power density as shown in **Figure S6** in the Supporting Information, similar to that in **Figure 2b**. The variation regular is same as the open-circuit voltage variation with the power density in **Figure S7** in the Supporting Information, indicating that the comprehensive pyro-phototronic effect can also sustained tuning the Schottky barrier beside inducing a transient current under a partial holding state.

The tuning role of comprehensive pyro-phototronic effect on the Schottky barrier is the result of light-induced secondary pyroelectric effect (i.e., thermal strain effect). The corresponding working mechanism is understood from the modification of the band diagram based on Anderson’s model as shown in **Figure 5**. The work function of Ag is about 4.26 eV

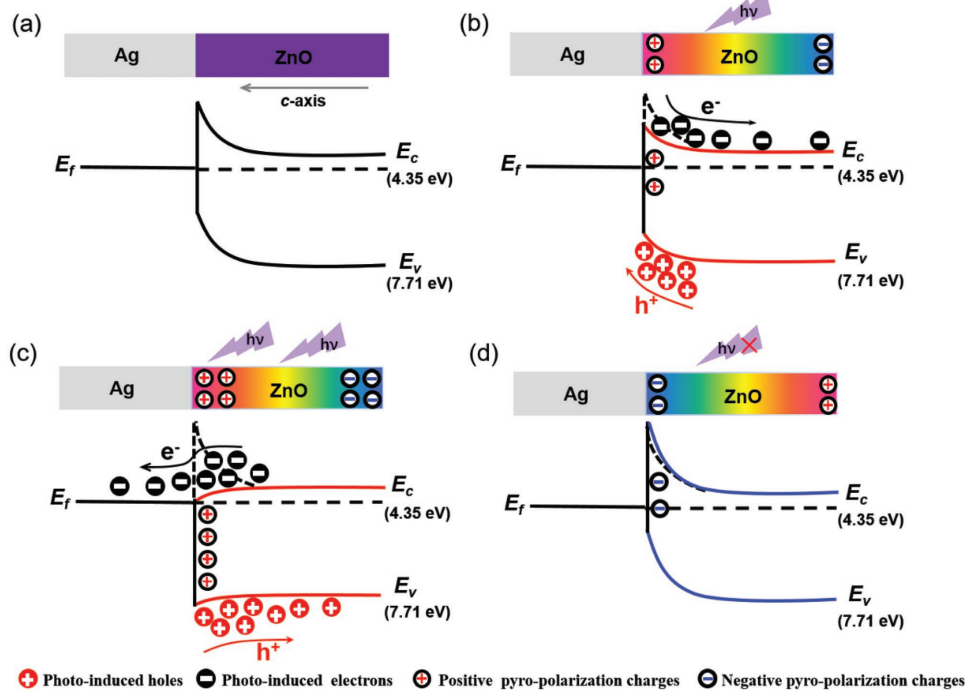


Figure 5. Working mechanism of the secondary pyro-phototronic effect on the steady-state current. a–d) Energy band diagrams of the flexible self-powered ZnO/Ag Schottky junction under the conditions of dark a), the weak illumination b), the strong illumination c), and withdrawing illumination d).

and the valence band and conduction band of ZnO (electron affinity ≈ 4.2 eV) are -7.71 and -4.35 eV versus vacuum.^[42,43] Under the dark condition in Figure 5a, a Schottky barrier is formed at the interface of ZnO NWs and Ag electrode. The *c*-axis direction of ZnO NWs points toward the silver electrode. Under a weak illumination of 325 nm, transient pyroelectric potential will be fast induced within the ZnO NWs, presenting an instantaneous photocurrent. At the same time, the temperature rise will also lead to a thermal deformation of the wurtzite ZnO crystal, and the same direction of the relative persist pyroelectric potential (named as the secondary pyroelectric potential) is also generated within the ZnO NWs by thermal strain effect and thus reduces the height of Schottky barrier at the interface shown as Figure 5b. The lower barrier height at the local Schottky contact means weaker built-in electric field and weaker photovoltaic effect. As a result, the secondary pyro-phototronic effect induced by the secondary pyroelectric effect of ZnO modifies and reduces the steady-state photocurrent of the fabricated PD, whose role is similar to the piezo-phototronic effect.^[44,45] As shown in Figure 5c, when the stimuli power density is increased up to 4.98×10^{-4} W cm⁻², the amount of positive relative persist polarization charges induced by secondary pyroelectric effect at the interface of ZnO/Ag becomes larger, resulting in a significant reduction of the Schottky barrier height, and the ZnO/Ag junction becomes the Ohm-like contact. And the steady-state current is near zero in the external circuit. When the power density is further increased, the barrier at the ZnO/Ag interface vanishes. The photogenerated electrons flow more easily from ZnO to silver electrode in the internal circuit, which is opposite from the former case with a weak illumination. When the illumination vanishing, the secondary polarization potential in ZnO NWs is opposite to the case under illumination as shown in Figure 5d. Negative pyroelectric polarization charges at the ZnO/Ag interface would increase the barrier height, resulting in a pyroelectric current from Ag electrode to ITO in the external circuit.

3. Conclusions

In summary, based on the ZnO/Ag Schottky structure, a flexible self-powered PD is successfully designed and achieved as showing the novel and unique features by using the comprehensive pyro-phototronic effect. First, the tuning mechanism of the primary and secondary pyro-phototronic effect on the transient and steady-state photocurrent is first demonstrated in the Schottky junctions, respectively. In particular, the overlooked secondary pyroelectric effect induced by UV illuminations is employed to sustainably modify the performances of PD by using the flexible substrate. This is a fundamentally new mechanism that relies on the naturally existing light-induced thermal strain effect of ZnO NWs. The Schottky barrier height is greatly tuned by the relative persist polarization charges induced by the light-induced thermal strain effect and the transport properties of the photogenerated carriers are thus modified within the Schottky junction, named as secondary pyro-phototronic effect. Moreover, this tuning approach is easily extended to other pyroelectric semiconductor-material-based optoelectronic devices and thus broaden its application fields. Second, a self-powered PD

on the flexible substrate is successfully achieved based on the ZnO/Ag Schottky junction. This configuration is easily obtained and provides high energy-efficient UV sensing. Third, the pyro-phototronic effect is used to significantly enhance the self-powered ZnO/Ag Schottky junction PD's performances under 325 nm illumination. The photocurrent of the PDs responding to 325 nm UV laser is improved by a maximal enhancement factor of ≈ 10 156% at a power density of 4.98×10^{-4} W cm⁻² thanks to the comprehensive pyro-phototronic effect. The specific detectivity and the responsivity of PDs are both enhanced by a maximal factor of 8371%. This work provides a potential approach to enhance/optimize the performances of Schottky junction-based optoelectronic devices by the pyro-phototronic effect and promising applications for ultrafast photo sensing, smart sensor, and wearable electronics.

4. Experimental Section

Fabrication Process of ZnO-Ag Schottky Junction PDs: The flexible PET substrate was cleaned by ethanol and distilled water. A thin layer of ITO and ZnO seed layer was deposited by radio frequency magnetron sputtering (Denton Discovery 635) at a power of 100 W for 1 h with the thickness of 100 nm. The coated PETs were then placed into the mixed solutions (0.06 M Zn(NO₃)₂ and 0.03 M hexamethylenetetramine) in a convection oven at 90 °C for 40 min. In order to get the separated ZnO NWs, 0–5 mL ammonium hydroxide (Aldrich) was added in per 60 mL mixing solution. Then a thin layer of Ag was deposited on ZnO NWs as the top electrode by direct current magnetron sputtering (Denton Discovery 635). Testing wires were connected to the top and bottom electrodes by silver paste, respectively. Finally, a thin layer of Kapton tape was used to fix the testing wires and improve their robustness.

Material Characterizations: Detailed microscopic structures of ZnO NWs were characterized by SEM (Hitachi SU4800). XRD patterns were collected using a Shimadzu XRD-6100 diffractometer with Cu α source ($\lambda = 0.154$ nm).

Optical and Electrical Measurements: Absorption spectra of ZnO were measured by a UV-vis spectrophotometer (SHIMADZU UV3600). *I*-*V* characteristics of the device were measured and recorded by a customized computer-controlled measurement system with Stanford SRS Low noise current preamplifier (SR570) and SRS Low noise voltage preamplifier (SR560) in conjunction with a GPIB controller (GPIB-USB-HS, NI 488.2). The optical input stimuli were provided by a He-Cd dual-color laser (Model No. IK57511-G, Kimmon Koha Co., Ltd.). A continuously variable filter was used to control the light power density. The corresponding power density was measured by a digital powermeter (Thorlab PM100D). An UV objective was used to expand 325 nm laser to illuminate the whole device in air. And the effective size of the device was 5 mm \times 5 mm.

Supporting Information

Supporting Information is available from the Wiley Online Library or from the author.

Acknowledgements

Y.W. and L.Z. authors contributed equally to this work. The authors thank U.S. Department of Energy, Office of Basic Energy Sciences (Award DE-FG02-07ER46394), the National Science Foundation (DMR-1505319), the National Natural Science Foundation of China (grant Nos. 11574033, 51432005, 11074024, and 11704032), Beijing cooperative

construction project, Beijing Higher Education Young Elite Teacher Project and the Fundamental Research Funds for the Central Universities for financial support.

Conflict of Interest

The authors declare no conflict of interest.

Keywords

pyro-phototronic effect, Schottky junction, secondary pyroelectric effect, self-powered, ultraviolet photodetector

Received: October 8, 2018

Revised: November 22, 2018

Published online:

-
- [1] E. Monroy, F. Omnès, F. Calle, *Semicond. Sci. Technol.* **2003**, *18*, R33.
 [2] S. M. Hatch, J. Briscoe, S. Dunn, *Adv. Mater.* **2013**, *25*, 867.
 [3] W. Y. Kong, G. A. Wu, K. Y. Wang, T. F. Zhang, Y. F. Zou, D. D. Wang, L. B. Luo, *Adv. Mater.* **2016**, *28*, 10725.
 [4] C. Soci, A. Zhang, B. Xiang, S. A. Dayeh, D. P. Aplin, J. Park, X. Y. Bao, Y. H. Lo, D. Wang, *Nano Lett.* **2007**, *7*, 1003.
 [5] Ü. Özgür, Y. I. Alivov, C. Liu, A. Teke, M. A. Reshchikov, S. Doğan, V. Avrutin, S. J. Cho, H. Morkoç, *J. Appl. Phys.* **2005**, *98*, 041301.
 [6] L. Zhu, L. Wang, F. Xue, L. Chen, J. Fu, X. Feng, T. Li, Z. L. Wang, *Adv. Sci.* **2017**, *4*, 1600185.
 [7] L. K. S. M, A. M, *Sensors* **2010**, *10*, 8604.
 [8] Y. Liu, C. R. Gorla, S. Liang, N. Emanetoglu, Y. Lu, H. Shen, M. Wraback, *J. Electron. Mater.* **2000**, *29*, 69.
 [9] S. Liang, H. Sheng, Y. Liu, Z. Huo, Y. Lu, H. Shen, *J. Cryst. Growth* **2001**, *225*, 110.
 [10] V. T. Tran, Y. Wei, H. Yang, Z. Zhan, H. Du, *Nanotechnology* **2017**, *28*, 095204.
 [11] Y. Dong, Y. Zou, J. Song, Z. Zhu, J. Li, H. Zeng, *Nano Energy* **2016**, *30*, 173.
 [12] J. Tang, B. K. Lee, A. J. Steckl, F. R. Beyette, *Proc. SPIE-Int. Soc. Opt. Eng.* **2000**, *4109*, 75.
 [13] M. E. Schaffer, P. A. Mitkas, *IEEE J. Sel. Top. Quantum Electron.* **1998**, *4*, 856.
 [14] Z. L. Wang, *Adv. Mater.* **2012**, *24*, 280.
 [15] P. Lin, L. Hu, X. Fang, *Adv. Funct. Mater.* **2014**, *24*, 2591.
 [16] Y. Yang, W. Guo, J. Qi, J. Zhao, *Appl. Phys. Lett.* **2010**, *97*, 9.
 [17] G. Cheng, X. H. Wu, B. Liu, B. Li, X. T. Zhang, Z. L. Du, *Appl. Phys. Lett.* **2011**, *99*, 203105.
 [18] Z. J., G. Y. H. Y. M. W. Y. PH, B. G. S. AK, P. DL, W. ZL, *Appl. Phys. Lett.* **2009**, *94*, R33.
 [19] X. Han, W. Du, R. Yu, C. Pan, Z. L. Wang, *Adv. Mater.* **2015**, *27*, 7963.
 [20] Z. Wang, R. Yu, X. Wen, Y. Liu, C. Pan, W. Wu, Z. L. Wang, *ACS Nano* **2014**, *8*, 12866.
 [21] T. H. Flemban, M. A. Haque, I. A. Ajia, N. Alwadai, S. Mitra, T. Wu, I. S. Roqan, *ACS Appl. Mater. Interfaces* **2017**, *9*, 37120.
 [22] Z. Bai, X. Chen, X. Yan, X. Zheng, Z. Kang, Y. Zhang, *Phys. Chem. Chem. Phys.* **2014**, *16*, 9525.
 [23] Y. F. Hu, J. Zhou, P. H. Yeh, Z. Li, T. Y. Wei, Z. L. Wang, *Adv. Mater.* **2010**, *22*, 3327.
 [24] Y. Zeng, X. Pan, W. Dai, Y. Chen, Z. Ye, *RSC Adv.* **2015**, *5*, 66738.
 [25] Z. Wang, R. Yu, X. Wang, W. Wu, Z. L. Wang, *Adv. Mater.* **2016**, *28*, 6880.
 [26] Z. Wang, R. Yu, C. Pan, Z. Li, J. Yang, F. Yi, Z. L. Wang, *Nat. Commun.* **2015**, *6*, 8401.
 [27] W. Peng, R. Yu, X. Wang, Z. Wang, H. Zou, Y. He, Z. L. Wang, *Nano Res.* **2016**, *9*, 3695.
 [28] W. Peng, X. Wang, R. Yu, Y. Dai, H. Zou, A. C. Wang, Y. He, Z. L. Wang, *Adv. Mater.* **2017**, *29*, 1606698.
 [29] M. Kumar, M. Patel, T. T. Nguyen, J. Kim, J. Yi, *Nanoscale* **2018**, *10*, 6928.
 [30] C. p. Ye, T. Tamagawa, D. L. Polla, *J. Appl. Phys.* **1991**, *70*, 5538.
 [31] H. S. Tzou, R. Ye, *Mech. Syst. Signal Process.* **1996**, *10*, 459.
 [32] J. D. Zook, S. T. Liu, *J. Appl. Phys.* **1978**, *49*, 4604.
 [33] X. A. Zhang, F. Hai, T. Zhang, C. Jia, X. Sun, L. Ding, W. Zhang, *Microelectron. Eng.* **2012**, *93*, 5.
 [34] A. Y. Polyakov, N. B. Smirnov, E. A. Kozhukhova, V. I. Vdovin, K. Ip, Y. W. Heo, D. P. Norton, S. J. Pearton, *Appl. Phys. Lett.* **2003**, *83*, 1575.
 [35] Y. Dai, X. Wang, W. Peng, C. Xu, C. Wu, K. Dong, R. Liu, Z. L. Wang, *Adv. Mater.* **2018**, *30*, 1705893.
 [36] Y. Luo, X. Yan, J. Zhang, B. Li, Y. Wu, Q. Lu, C. Jin, X. Zhang, X. Ren, *Nanoscale* **2018**, *10*, 9212.
 [37] D. Periyangounder, P. Gnanasekar, P. Varadhan, J.-H. He, J. Kulandaivel, *J. Mater. Chem. C* **2018**, *6*, 9545.
 [38] G. Konstantatos, E. H. Sargent, *Nat. Nanotechnol.* **2010**, *5*, 391.
 [39] X. Liu, L. Gu, Q. Zhang, J. Wu, Y. Long, Z. Fan, *Nat. Commun.* **2014**, *5*, 4007.
 [40] Y. Feng, Y. Zhang, Y. Wang, Z. Wang, *Nano Energy* **2018**, *54*, 429.
 [41] R. W. Whatmore, *Rep. Prog. Phys.* **1986**, *49*, 1335.
 [42] L. J. Brillson, Y. Lu, *J. Appl. Phys.* **2011**, *109*, 121301.
 [43] J. A. Aranovich, D. Golmayo, A. L. Fahrenbruch, R. H. Bube, *J. Appl. Phys.* **1980**, *51*, 4260.
 [44] Y. Yang, W. Guo, K. C. Pradel, G. Zhu, Y. Zhou, Z. Yan, Y. Hu, L. Long, L. W. Zhong, *Nano Lett.* **2012**, *12*, 2833.
 [45] Z. L. Wang, G. Zhu, Y. Yang, S. Wang, C. Pan, *Mater. Today* **2012**, *15*, 532.